

HIGH RESOLUTION PHOTOELECTRON SPECTROSCOPY OF SOLIDS



Ammu Mathew (CY10D021)

Anirban Som (CY10D022)

Radha Gobinda Bhuiin (CY10D047)

Amitava Srimany (CY11D004)

Krishnadas K R (CY11D016)

INTRODUCTION:

Photoelectron spectroscopy is based on the phenomenon called 'photoelectric effect', first observed by Heinrich Hertz in 1887. In this effect, electrons are emitted from certain metals, when their surface is exposed to suitable electromagnetic rays. Albert Einstein, in 1905, presented a theoretical explanation¹ for this effect based on the Max Planck's quantum theory of radiation. Early experimental observations on this effect and Einstein's mathematical explanations form the basis for the versatile experimental tool called photoelectron spectroscopy.

Basically, an experiment in photoelectron spectroscopy involves exposure of the sample to suitable monochromatic radiation and observation of the emitted electrons called photoelectrons. Mainly, there are three characteristics by which photoelectrons can be analyzed: their kinetic energy, directions of emission with respect to the sample and exciting radiation and the orientations of the spin. Three basic photoelectron spectroscopic techniques were developed based on the measurements of these properties. Most common technique among these involves the measurement of the number distribution of photoelectrons with their kinetic energy. Another two techniques involve the measurement of photoelectron intensity distribution as a function of either the angle of emission or spin distribution. The latter two techniques are much more complex than kinetic energy analysis and hence, it is the most widely used technique in photoelectron spectroscopy. As proposed by Einstein, the relation between the energy of the incident radiation and the kinetic energy of the photoelectrons is described by the photoelectric equation:

$$h\nu = E_b^{\vee}(k) + E_{kin}.$$

where $E_b^{\vee}(k)$ is the binding energy or ionization potential of the k^{th} level as referred to the vacuum level and E_{kin} is the photoelectron kinetic energy.

There are, generally five techniques collectively called as electron spectroscopy: they are x-ray photoelectron spectroscopy (XPS), ultraviolet photoelectron spectroscopy (UPS), Auger electron spectroscopy (AES), electron energy loss spectroscopy (EELS), and inverse photoemission spectroscopy (IPS). Here, we discuss certain applications of XPS and UPS with emphasis on their resolution. We describe the factors affecting the energy resolution of these techniques when applied to studies on solids, recent developments in enhancement of energy resolution.

ENERGY RESOLUTION IN PHOTOELECTRON SPECTROSCOPY

Here, resolution can be energy resolution or spatial resolution. We describe here the factors affecting the energy resolution in photoelectron spectroscopy, techniques to improve it and present some examples of the applications of such high resolution techniques. In the case of XPS, the overall energy is given approximately by, $(\Delta E = \Delta E_x^2 + \Delta E_A^2 + \Delta E_2^2)^{1/2}$, where ΔE_x is the FWHM of the X-ray line, ΔE_A is the width of the energy analyser window, ΔE_2 is the natural line width of the orbital of the atom². ΔE_2 is fixed and ΔE_A can be adjusted so that it does not affect the resolution. Then the resolution is controlled by the width of the x-ray line alone. In XPS, most commonly used x-ray sources are Mg K α and Al K α with natural line widths of 0.75 and 0.85 eV, respectively. Using a suitable monochromator, we can reduce the line width of the x-ray source. It is to be remembered that reduction of the line width naturally decreases the intensity of the signal. The best energy resolution available to date, for commercial XPS instruments, is 0.28 eV using a monochromator with Al anode. One of the ways to achieve better resolution is to replace these conventional sources with synchrotron or x-ray lasers. Resolution is obtained by measuring the width of a narrow core line or the width of the Fermi edge of a noble metal at low temperatures. Generally the 4f line of metallic Au or the valence p level in a rare gas is measured.

NEED OF HIGH RESOLUTION PHOTOELECTRON SPECTROSCOPY OF SOLIDS

Photoelectron spectroscopy is a versatile tool for studying the electronic energy levels of atoms, molecules, solids and their surfaces. PES measurement with high energy resolution is an essential tool for investigating some interesting phenomena in solid state physics. The electronic structures of the bulk of a solid can be different from those in the surface region, due to surface reconstruction or relaxation and electron correlation effects. Band structure measurements or Fermi surface maps of solids require an energy resolution of about 50 meV. But, for studying the many-body effects in photoemission spectra requires an energy resolution of at least one order of magnitude better than this.

Fine spectral features of solids near the Fermi level are directly related to low energy excitations in the material. A quantitative study of these fine spectral features requires very high resolution measurements. Investigations on some physical properties of solids, such as superconductivity and magnetism require high absolute energy resolution. For example, for a study of the high-T_c superconductivity, with a superconducting gap of 20 meV, energy resolution should be

better than 20meV. In the case of a conventional superconductor like Pb (superconducting gap ~ 3 meV), synchrotron radiation, with a resolution of less than 1 meV, has been used.

EXAMPLES OF HIGH RESOLUTION PES OF SOLIDS :

EVIDENCE FOR GAP ANISOTROPY IN AN f-ELECTRON SUPER CONDUCTOR³ :

One of the applications of high resolution photoelectron spectroscopy is in the study of superconductors. Since photoelectron spectroscopy is highly surface sensitive, it cannot provide reliable data for f-electron superconductors which exhibit a surface electronic structure, different from the bulk. Due to the extremely small energy scale of these f-electron superconductors, very high resolution photoelectron spectroscopic studies are needed. Here, a vacuum ultraviolet laser (6.994 eV) with a sub-meV energy resolution has been used for measuring the superconducting gap of CeRu₂. It is demonstrated that laser-PES can be used for directly and precisely studying the intrinsic bulk superconductive electronic structure of correlated f- and d-electron superconductors with energy scales less than 1 meV. Schematic of the spectrometer used is shown below.

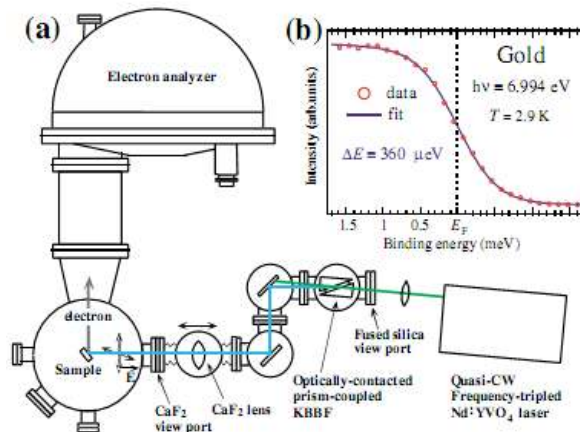


Figure 1. (a) Schematic of the PES spectrometer used and (b) ultra high resolution PES spectrum of an evaporated Au film measured at 2.9 K together with the calculated spectra.

The second harmonic of a quasi-CW frequency tripled Nd:YVO₃ laser by using an optically contracted prism coupled KBe₂BO₃F₂ crystal is focused on a sample with a CaF₂ lens. Kinetic energies of photoelectrons are measured using a high precision hemispherical energy analyzer (GAMMADATA SCIENTA R-4000). Though the use of a laser as photon source is not new, the combination of a high-resolution energy analyzer and a quasi-continuous laser system using a nonlinear crystal system is

unique. Figure 1b shows the ultra high resolution measurement of a gold Fermi edge spectrum measured at 2.9 K. It shows a good correspondence to the convolved Fermi-Dirac function, indicating the energy resolution of 620 μeV . Figure 2a shows the temperature-dependent ultrahigh resolution PES spectra of high quality CeRu_2 single crystal across T_c measured with a total energy resolution of 520 μeV .

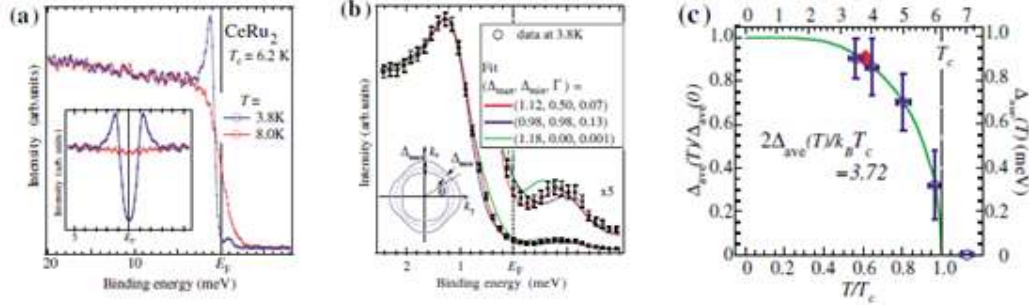


Figure 2. Ultra high resolution PES data of CeRu_2 . (a). Temperature-dependent spectra near E_f with an inset showing the symmetrised spectra from the same data. (b). Normalized SC DOS at 3.9 K with a calculated spectra. (c). T-dependent SC gap values.

The spectrum at 8 K has a Fermi edge while, that at 3.8 K shows a sharp peak at 1.35 meV with a leading-edge shift to higher binding energy, which indicates the opening of the SC gap. The small peak above E_f of the SC spectrum corresponds to thermally excited electrons across the gap. The formation of the gap across T_c is more clearly seen in the inset. Figure 2b shows the normalized SC spectrum, compared with three calculated spectra with $(\Delta_{\max}, \Delta_{\min}, \Gamma) = (0.98, 0.98, 0.13)$, isotropic case), $(1.12, 0.50, 0.90)$, anisotropic case), and $(1.18, 0.00, 0.001)$, maximum anisotropy) in units of meV. From Figure 2c, it is clear that, the obtained Δ_{ave} . for different samples in the present studies agree well with each other within the experimental accuracy. Present success in probing the bulk superconducting electronic states of CeRu_2 opens up important opportunities in solid state physics. This technique can be applied to any other material having differing surface and bulk electronic states. In conclusion, ultra high resolution PES using a laser as a photon source has been proven to be useful for the measurement of bulk SC gap of an f-electron superconductor.

HIGH RESOLUTION LOW ENERGY PHOTOELECTRON SPECTROSCOPY WITH THE USE OF A MICROWAVE EXCITED RARE GAS LAMP AND IONIC CRYSTAL FILTERS⁴:

Discharge lamps using He, Ne and other rare gases were traditionally used for PES measurements. The self-absorption and Doppler broadening could not realize the energy resolution better than 1 meV. Hence, lower pressures and slower thermal motions are required for obtaining extremely narrow line width from rare gas light source. To rectify this problem, rare gases under low

pressures are taken in a small ceramic tube, excited by microwave, and kept under an external magnetic field. Three strongest lines at three different energies are easily extracted with high efficiency using proper ionic crystal filters. The energy resolution, better than 600 μeV was achieved.

Light source: The gas (Xe, Kr or Ar) is excited by microwave in the small ceramic tube by means of electron-cyclotron resonance plasma, emits light through a metal aperture of 2 mm in diameter. The pressure is kept in the middle 10^{-3} torr range during the operation. Unnecessary gas is pumped out to reduce self-absorption and to get narrower line width of the strongest emission line. The strongest lines obtained from Xe, Kr and Ar are 8.4, 10.0 and 11.6 eV, respectively.

Filter: The emitted light is composed of many lines at different energies. To obtain the monochromatic light, a grating or a filter. In order to use only the strongest line emitted by the source, it is practical and inexpensive to use ionic crystal filters like sapphire, CaF_2 , LiF, etc. By changing the temperature we can eliminate high energy components by the exciton absorption or the Urbach tail. A semiconductor heater is used to heat up the LiF filter and the temperature of the filter is measured by a thermocouple. Schematic view of the optical system is shown below.

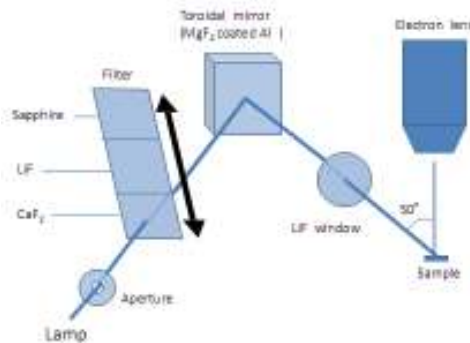


Figure 3. Schematic view of the optical system used.

LOW ENERGY PHOTOELECTRON SPECTROSCOPY OF A HEAVY FERMION MATERIAL:

The experimental set up shown above is used for angle integrated extremely low energy PES (ELEPES) measurements of LiV_2O_4 , which is known as a heavy fermion material. Upper panel of Figure 4 shows the results of measurements at 3 K at an energy of 8.4 and 10.0 eV, where a total energy resolution better than 4 meV is achieved. In the lower panel, all spectra at different temperatures cross the E_f at the intensity noticeably higher than half of the Fermi edge. This suggests the presence of higher density of states above E_f . Since the photoionisation cross section is much stronger for the O 2p component relative to the V 3d component, at these low energy, it is understood

as the O 2p density of states (DOS) is slightly decreasing toward the E_f , whereas the V 3d component increasing toward and beyond the E_f . If the ELEPES is divided by the Fermi-Dirac distribution function, DOS can be evaluated beyond the E_f . Then a slight peak is seen in this case around -10 eV, which is ascribed to the DOS of the O 2p states hybridized with the V 3d components. Such hybridized states may be responsible for the heavy fermion behavior of this material. Thus it is understood that ELEPES is reflecting the bulk properties in this material.

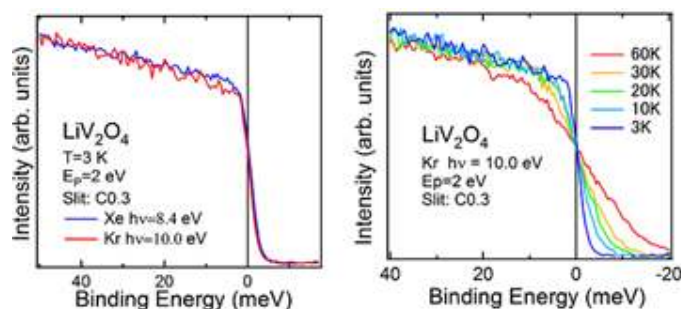


Figure 4. ELEPES of fractured clean surface of LiV_2O_4 at 3K (upper panel). The temperature dependence is shown in the lower panel.

ANALYSIS OF THE INTERFACE OF LONG CHAIN ALKANETHIOL AND Au (111) SUBSTRATE⁵:

Two main models are used to describe thiol binding to Au(111) surface forming SAMs. According to the earlier model, thiol headgroups sits in either a hollow site⁶ or in a bridging site⁷ on a unreconstructed Au(111) surface. The other model suggests binding of thiol groups to an Au adatom present on Au(111) surface, which appear as a result of adsorbate-induced surface modification. STM studies on methylthiolate (C1S) reveals formation of adatom-thiolate complexes where the adatom seats on bridging site on Au(111) and S headgroups of C1S species binds towards the side of the adatom and sits on atop site of underlying Au(111) surface⁸.

Au 4f HRXPS emission signal from clean Au(111) can be decomposed into two components corresponding to surface(S_c) and bulk(B) atoms⁹. The possible shift and branching of the surface component in Au(111) HRXPS can be monitored and bond strength and charge transfer associated with headgroup-substrate bond formation can be estimated. A downward shift of the 0.25 eV in Au 4f component has been observed upon SAM formation with C12S¹⁰. The Au 4f_{7/2} spectra obtained for butylthiolate(C4S) on single crystal Au(111) exhibit one single emission peak which is decomposable into three components – bulk feature(B), shifted surface component (S_T) and an additional shoulder(T) towards higher binding energy¹¹. This shoulder is possibly due to the Au atoms directly bonded to the Au headgroup atoms whereas the shifted surface component (S_T) is due to the Au atoms indirectly

affected by thiol binding. For C4S S_T/T ratio has been found to be 3.1 which is on a par with theoretical value of 3:1 for directly bonded: indirectly affected Au atoms for adatom-monothiolate bonding configuration. To what extent this model can be extended to long chain alkanethiols has been a controversial issue though. To cast further light into this problem several HRXPS experiments has been performed with dodecanethiolate(C12S) as long chain AT SAM and with hexanethiolate(C6S) as intermediate chain AT SAM on Au(111) surface.

The substrates for SAM preparation were mica slides with an 300 nm thick Au(111) layer. SAMs were prepared by immersion of the substrate in 1mM ethanolic solution for 24 hour at room temperature or at 72°C.

The HRXPS measurements were performed at beamline D1011 of MAX-lab synchrotron radiation facility in Lund University, Sweden. Maximum surface sensitivity was ensured by optimizing the photon energy. The energy resolution was 50-70 meV. The HRXPS spectra were fitted by symmetric Voigt functions and either Shirley-type or linear background using XPS Peak 4.1 program.

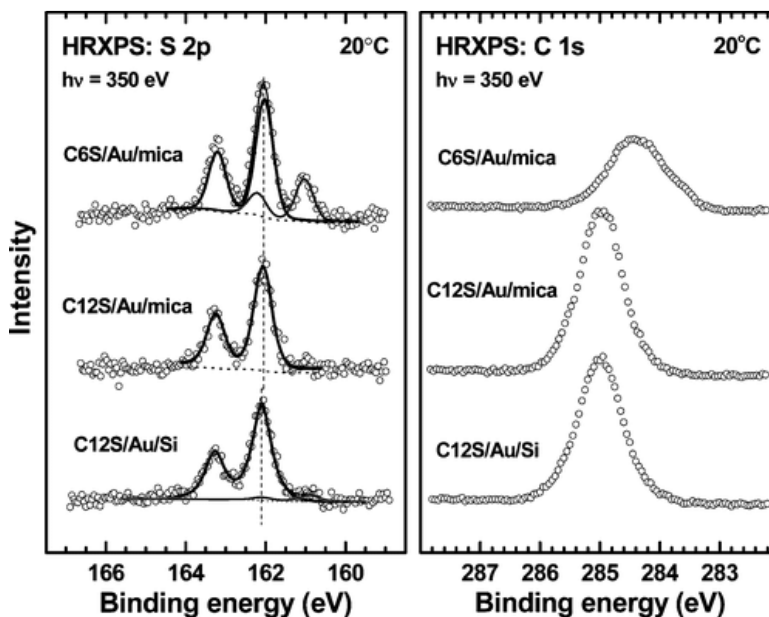


Figure 5. HRXPS spectra of S 2p (left panel) and C 1s (right panel) for C6S/Au/mica, C12S/Au/mica and C12S/Au/ Si acquired at a photon energy of 350 eV. SAMs were prepared at room temperature.

S 2p spectra in Fig.5 comprises of a dominant doublet at BE of about 162.05 eV which can be assigned to thiolate S bonded to Au. For C12S in Fig.5 the doublet is the only feature suggesting that all the thiolates are attached to the substrate in the same manner. For C6S there are actually two doublets, additional one being at BE of about 161.0 eV. This is possibly due to another type of thiolate sulphur

with different binding chemistry. Another feature in this spectra is smaller fwhm for films Au/mica (0.50 eV) than on Au/Si (0.58) and this is the manifestation of highly homogeneous AT film formation on Au/mica.

Apart from the difference in intensities, for C1S spectra, both binding energy and fwhm for C12S and 6S are distinctly different. Two different BE (284.95 and 284.4 eV) for two different AT SAMs is due to screening of photoemission hole by the conduction electrons of substrate, an effect decreases with distance between the excitation site and the substrate. The same effect contributes to the larger fwhm too. In case of C6S film there is a shoulder in the C1S spectra which is due to α -carbon¹².

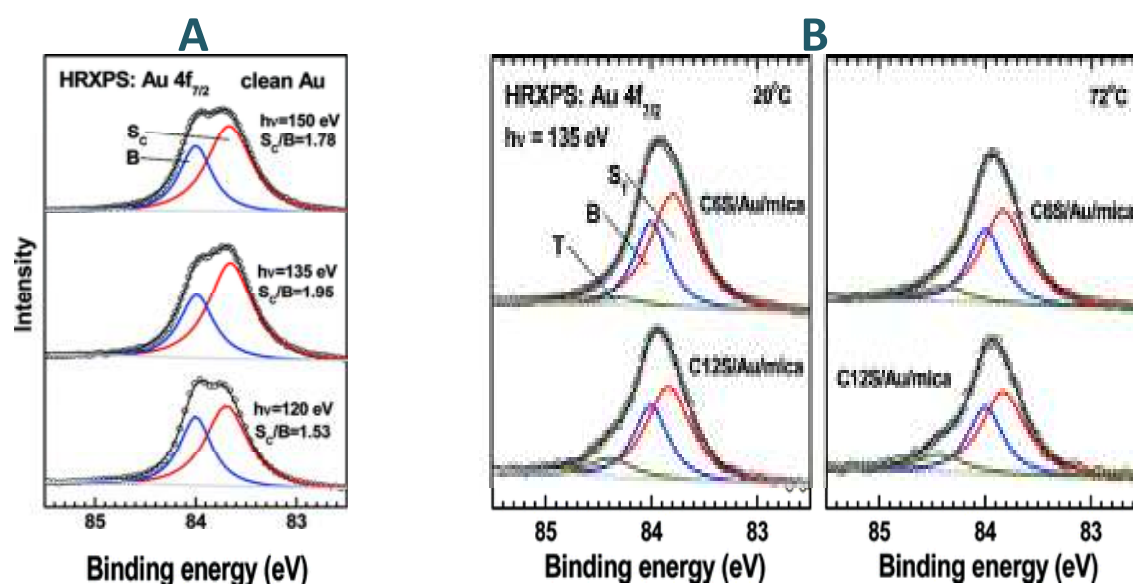


Figure 6 (A) Au 4f_{7/2} HRXPS spectra of clean Au surface acquired at photon energies 120, 135 and 150 eV. In each cases the spectra are decomposed into the bulk (B; blue trace) and surface (S_c; red trace). (B) Au 4f_{7/2} HRXPS spectra of C6S/Au/mica and C12S/Au/mica prepared at 20°C (left panel) and at 72°C (right panel). The spectra are decomposed into the bulk (B; blue line), and two surface (S_T and T; red and green trace respectively) components.

Acquisition geometry and the photon energy were optimized using a clean gold sample prior to Au 4f_{7/2} HRXPS measurements on the SAMs. Softly sputtered Au(111) on mica was used for this purpose. Au 4f_{7/2} spectra acquired on clean Au surface at photon energies 120, 135 & 150 eV is presented in Figure 6A. The general feature of the spectra represents an asymmetric single peak which can be explained in terms of two merged peaks whose relative intensity varies as a function of incident photon energy. These two peaks are actually associated with gold atoms in bulk (B) and on the topmost layer (S_c). For all these studies normal emission geometry with an acceptance angle of $\pm 7^\circ$ was used,

the incident angle of the primary X-ray source was 40° and only the photon energy was varied. For further investigation of Au $4f_{7/2}$ from the SAMs photon energy of 135 eV was chosen as it gives the highest resolution for Surface atoms (S_c). The Au $4f_{7/2}$ HRXPS spectra of the prepared AT films are given in Fig. 6B. Attachment of thiols to the surface results in splitting of the S_c component into higher binding energy T and lower binding energy S_T components. The shift in S_T with respect to S_c was +0.18 eV. These parameters are close to the values obtained for C4S and C1S but not absolutely identical. The most important difference is the difference in intensity between shifted surface component and the shoulder (S_T/T). This was found to be around 3 for C4S and C1S previously, but for C12S it has been found to be around 5 and for C6S a value of 15 has been obtained.

The exact structure of the interface seems to be different for the short chain and long chain AT SAMs. The S_T/T ratio which is considered to be the fingerprint for different adsorption models has been found to be quite different for the long chain thiols than the values reported for the short chain counterparts. At this moment this is not very clear though whether this difference is significant and new model is required or not but the data provides strong evidence about the presence of adatoms at the interface between AT headgroups and Au(111) substrate.

RECONSTRUCTION OF MOLECULAR ORBITAL DENSITIES FROM PHOTOEMISSION DATA¹³:

To investigate the band structure of solids by measuring the kinetic energy versus angular distribution of the photo-emitted electrons, photoemission spectroscopy is a useful tool. Discrete orbitals of large π -conjugated molecules can be characterized by using this experimental technique. From the measurement of photoemission intensity in constant initial-state energy over a hemispherical region, it can be generated reciprocal space maps of the emitting orbital density. The real-space electron distribution of molecular orbitals in both a crystalline pentacene film monolayer obtained from a simple Fourier transform of the measurement data is presented here. It has been shown that the result obtained from experiment is in good agreement with density functional calculations.

For a compound's information about chemical, electronic, and optical properties can be obtained from its highest occupied and lowest unoccupied electronic orbitals. The electronic states are depicted by band structures for extended periodic systems, for given momentum values k the allowed energies is E , and the orbitals are Bloch wave functions associated with a particular k point. For molecules, the orbitals are looked at as a particular spatial distribution of the electron density at discrete energies. Imaging of molecular orbitals is possible by using various experimental techniques under certain conditions¹⁴ such as femtosecond laser pulse¹⁵, electron momentum spectroscopy¹⁶, and

scanning tunnelling microscopy¹⁷. Nevertheless, strong bonding interactions with the substrate complicate interpretation of the images¹⁸, for which a more reliable experimental technique is needed. In this case by using ultraviolet angle-resolved photoelectron spectroscopy (ARPES), it has been established molecular orbital densities to be reconstructed in real space in a simple way, as illustrated by analysis of a crystalline pentacene film and a chemisorbed monolayer, *P*-sexiphenyl on Cu (110).

An ARPES set up is schematically represented in Fig. 7 in which an incident photon of energy $h\nu$ excites an electron from a bound initial state, represented by wave function Ψ_i and energy E_i , to a final electron state Ψ_f with kinetic energy E_{kin} . In the photoemission process energy and momentum are conserved, from the measurement of energy and momentum of the emitted electron probes the band structure of solids. To investigate the band dispersions, Fermi surface and many-body-correlation in a wide range of materials ARPES is commonly used¹⁹.

The PE intensity is represented by a Fermi golden rule formula²⁰

$$I(\theta, \phi; E_{kin}) \propto \sum_f |\langle \Psi_f(\theta, \phi; E_{kin}) | \mathbf{A} \cdot \mathbf{p} | \Psi_i \rangle|^2 \times \delta(E_i + \Phi + E_{kin} - h\omega)$$

Here, θ and ϕ are the polar azimuthal emission angles respectively as represented in Fig. 7 and to ensure energy conservation delta function is used, where Φ denotes the sample work function. And momentum operator and vector potential operator are represented by \mathbf{p} & \mathbf{A} . In the above equation only difficulty is calculation of the final state, for which approximation is taken in which it is considered as a plane wave (PW) character only by the direction and wave number of the emitted electron²¹. It is the first presented result for the organic π -conjugated molecular semiconductor pentacene in a multilayer thin film. Pentacene is a planar aromatic molecule consisting of five linearly edge-fused phenyl rings. By using both PE experiments²²⁻²⁴ and density functional theory (DFT)²⁵⁻²⁷, intermolecular HOMO dispersion of pentacene has been analyzed. Crystalline pentacene (022) films²⁸ (Fig. 7C) were prepared on the $p(2 \times 1)$ oxygen reconstructed Cu (110) surface by vacuum deposition, in which π face tilted out of the surface plane by an angle of $\beta = 26^\circ$. A momentum map at the HOMO energy of a pentacene multilayer has been shown in Figure 7D using a toroidal electron energy analyzer at the synchrotron radiation facility BESSY II²⁹.

There is a pronounced intensity maximum of the PE intensity along k_x , which is a function of the momentum vector parallel to the molecular axis at 1.15 \AA^{-1} , as observed previously and along k_y it is

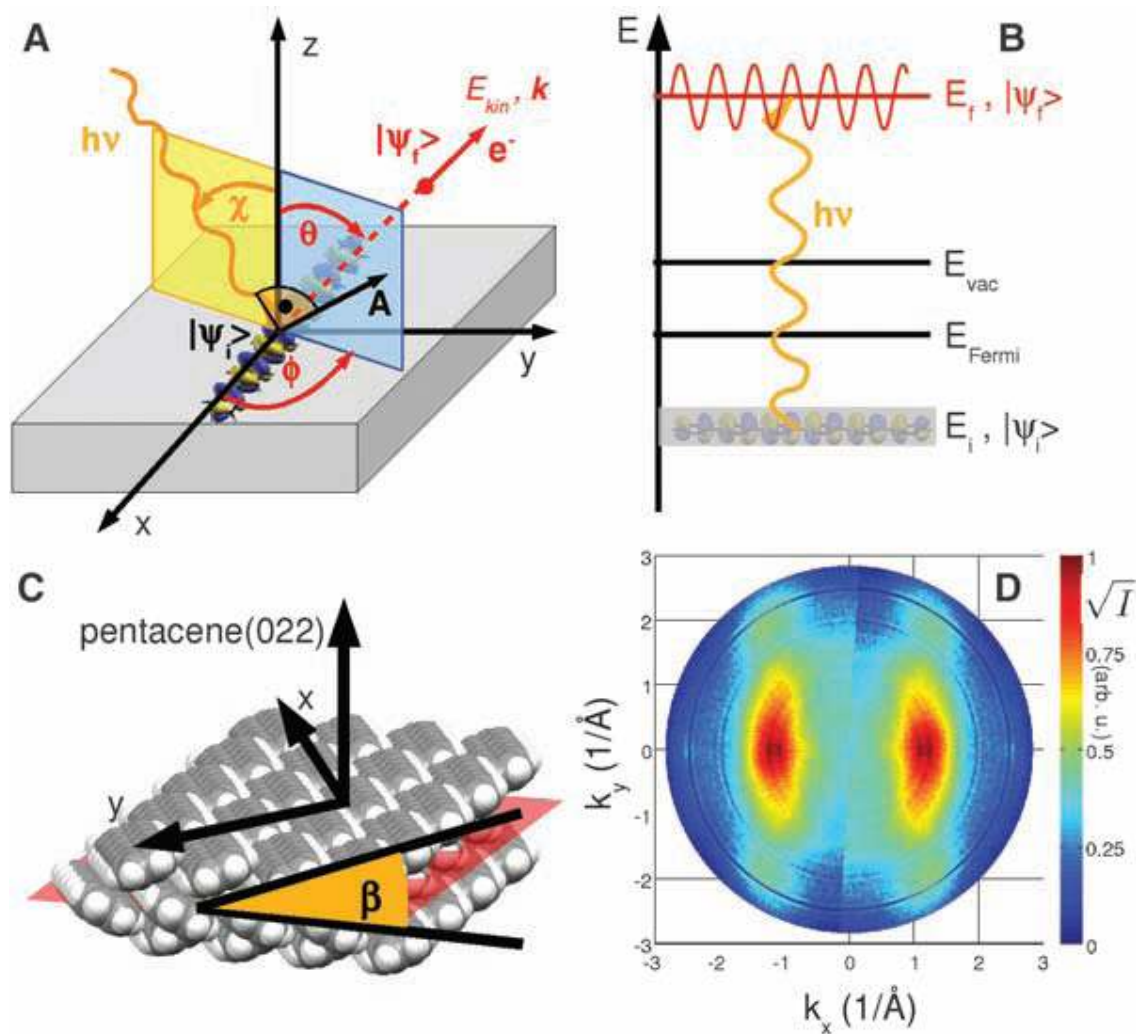


Figure 7. Momentum maps in angle-resolved PE experiments. (A) The incident photon with energy $h\nu$ and vector potential A excites an electron from the initial state Ψ_i to the final state Ψ_f characterized by the kinetic energy E_{kin} and the momentum vector k . The polar and azimuthal angles θ and ϕ , respectively, define the direction of the photoemitted electron. (B) Schematic energy-level diagram showing the energy of the initial state E_i , the Fermi level E_{Fermi} , the vacuum level E_{vac} , and the final-state energy E_f . (C) Model of the pentacene multilayer arrangement on a Cu (110)-(2 \times 1) O surface: The long molecular axis points along the x axis, and the (022) surface (indicated by the red plane) features pentacene molecules tilted by $\beta = 26^\circ$ out of the xy plane. (D) Square root of the PE intensity as a function of azimuthal and polar angle after conversion to momentum (azimuthal scan) at a constant binding energy of 1.3 eV ($h\nu = 35$ eV) corresponding to the pentacene HOMO.

extend about $\pm 0.8 \text{ \AA}^{-1}$ in the momentum maps. In addition, there are weaker intensity lobes at about the same k_x value around $k_y \approx \pm 2 \text{ \AA}^{-1}$.

To compare with the theoretical data, DFT calculation has been done for the same and resulting HOMO orbital is described in Figure 8A and corresponding three-dimensional FT in Figure 8B. Ft is measured on a hemisphere of radius $k = \sqrt{(2m/h^2)E_{kin}}$ since momentum maps is evaluated at constant binding. In Figure 8C the value of the FT on that hemisphere is shown for the kinetic energy of 29.8 eV. There is a discrepancy with this calculated value from the photoemission data (Fig 7D). This is due to geometric case, presence of both $+26^\circ$ and -26° tilt angle β in the film structure. If this has to be considered, theory result gives a good agreement with the experimental value. Both results from the out-of-plane tilt angle of the pentacene molecules shows the strong maximum at $k_y = 0$ and the weak peaks at $k_y = 2 \text{ \AA}^{-1}$. The ARPES approach is estimated the accuracy to be better than 5° . Furthermore, ARPES works at low photon energy, so minimum damage of the sample and no need to have a tunable photon source.

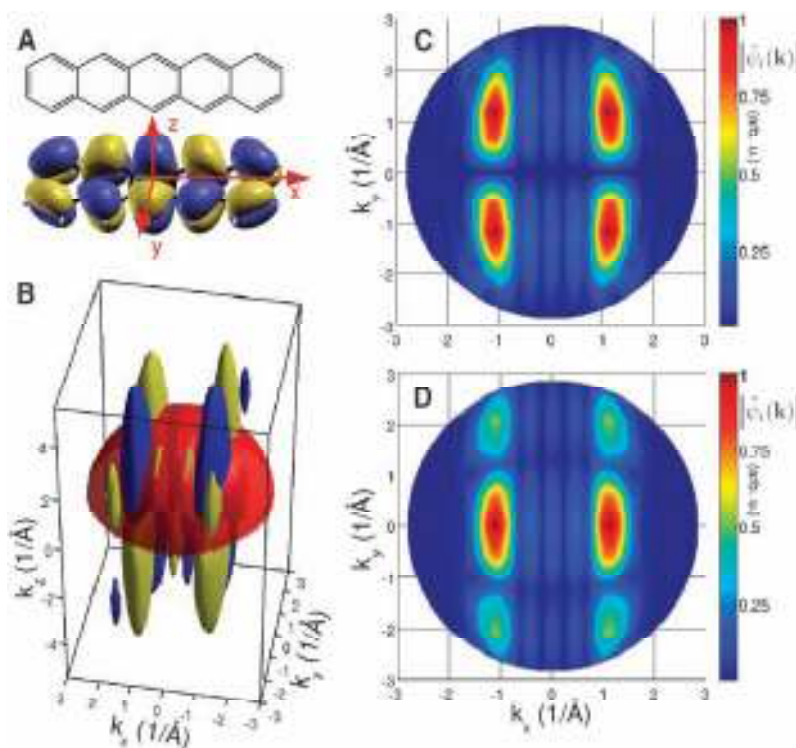


Figure 8. Calculation of the PE intensity from the FT of the molecular orbital. (A) Line drawing and HOMO of pentacene as obtained from a DFT calculation for an isolated molecule. The choice of the coordinate system is indicated, where x and y are parallel to the long and short molecular axis, respectively, and z is perpendicular to the molecular plane. (B) Three-dimensional FT of the HOMO as an isosurface plot; blue indicates negative and yellow, positive values, together with a hemisphere of radius $k = \sqrt{(2m/h^2)E_{kin}}$ with a kinetic energy $E_{kin} = 29.8 \text{ eV}$. (C) Absolute value of the HOMO FT on the hemisphere shown in (B). (D) Simulation of PE intensity of the pentacene multilayer film, taking into account molecules with tilt angles of $\beta = +26^\circ$ and $\beta = -26^\circ$ out of the xy plane.

NEW INSTRUMENTATIONAL DEVELOPEMENT:

To get accurate information about the orbital energies or binding energies of solid materials through photoelectron spectroscopy, it is very important to use a high resolution instrument. Without high resolution instrument it is very difficult to resolve the closely lying vibrational energy states. Resolution of an instrument can be affected by various parts of the instrument, namely the photon source, analyzer and the detector also. For solid samples one more factor affects the resolution of the spectrum and that arises due to the fact that every radiation, depending upon the energy, have some penetration depth into the samples and as a consequence the photoelectrons coming out of the inner layers of the samples loses some energy with the loss of exact information about the orbital it has been generated from. To develop high resolution instrument it is necessary to avoid the problems occurring from the above mentioned facts.

The photon source is the first and one of the important things to be considered to increase the resolution of the instruments. It is one of the primary reasons for the peak broadening in the spectra and destroys the fine structures of the spectra and we lose the information about the vibrational states of molecules. To minimise problems associated with the light source it is absolutely necessary to obtain purely monochromatic light from the source and extremely small pulse width. The last decade have shown tremendous development in this field and as a result synchrotron radiation source and modern high harmonic gain laser sources have been developed in recent past and they are the promising sources to obtain highly monochromatic pulsed radiation and used in modern high resolution spectrophotometers.

To the date most of the high resolution instruments have a hemi-spherical electrostatic analyzer and this type of instrument show highest energy resolution³⁰. For high kinetic energy photoelectron spectroscopy, instrument with this kind of analyzer have achieved resolution in the order of 10^5 ³¹. But the luminosity of the instrument with this kind of analyzer having a typical 0.1 mm entrance slit is low. To get increased luminosity time of flight (TOF) type of analyzer can be used. But this kind of analyzer have lower energy resolution. To get benefit of both the luminosity and resolution a new kind of analyzer, known as ARTOF 10k (Fig. 9), has been developed very recently which combines TOF technology with electron lens systems of photoelectron spectrometers³².

The electrons coming out of the samples enters into the analyzer. All the electrons within a cone of 30° opening angles enters into the analyzer which accounts for the higher luminosity of the instrument. The analyzer consists of 5 lens elements. When electrons enter into the analyzer, the applied negative voltages in the electron lens causes the retardation of the electrons and increases

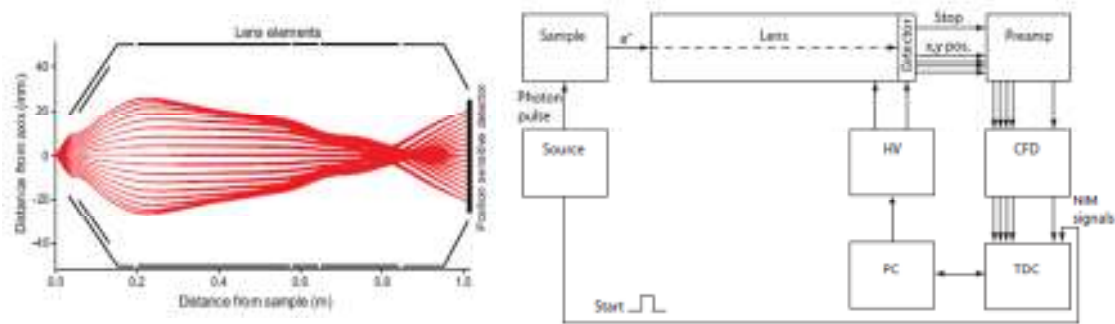


Figure 9. Simulated trajectories of electrons through the ARTOF flight tube (left) and the schematic of signal flow in the instrument (right).

the flight time. As a result energy resolution of the instrument increases. After passing through the analyzer the electrons hit the detector. The detector accepts electron for a specified time window with certain kinetic energy of the electrons. This cut-off acceptance increases the resolution of the measurement. The detector used with this instrument is a position-sensitive delay-line detector. This detector is able to accurately measure the flight time (t) of the photoelectrons that are coming through the analyzer and the exact position (x,y) where it hits the detector. Now a transformation matrix can be used to obtain the kinetic energy (E_k) values of the electrons and the angular parameters (φ, θ). Hence the position of the origin of each of the electrons can be determined.

For the first measurement using this instrument a gold wire has been taken as sample. In front of this a pepper-pot type patterned foil was placed to distinguish the angular distribution of the electrons and to characterize the instrument performance for angular resolution. After getting data in (x, y, t) space, it has been transformed to (θ, φ, E_k) using a transformation matrix. The three dimensional

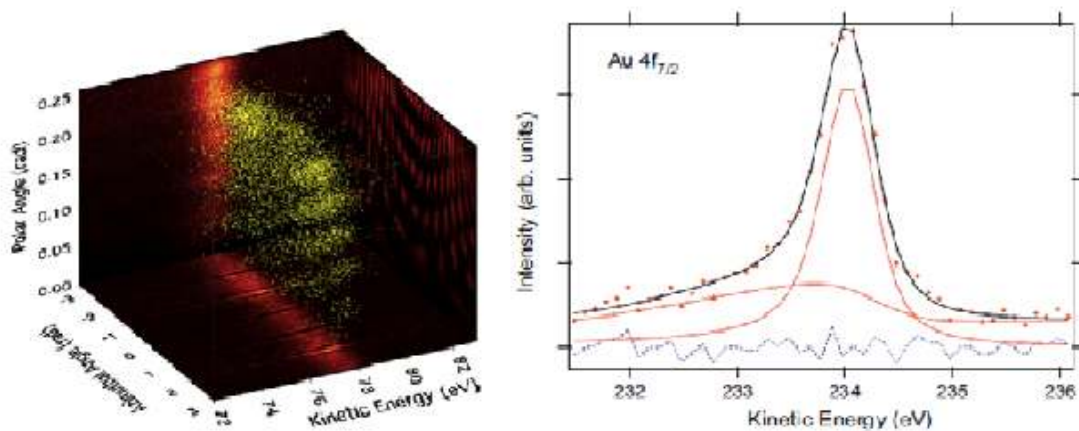


Figure 10. 3D representation of the C1s peak in (θ, φ, E_k) space (left) and angle integrated electron spectrum of Au 4f_{7/2} line (right).

representation of the C1s peak has been shown in the figure 10 (left). Carbon is coming as a contamination in the surface. Similarly data have been recorded for Au 4f_{7/2} and the angle integrated spectrum have been shown in the figure 10 (right). The red lines are Doniach-Sunjic and Shirley profiles used in the fit and the dashed line is the residue. Resolution obtained in this measurement is around 0.35 eV which is not very good. The photon bandwidth for this experiment was 0.1 eV. The majority of the broadening is believed to be coming from the uncertainty in the trigger electronics. This can be avoided by improving the electronics and optimizing various parameters of the set up and theoretically simulated values, which is in the order of meV, can thus be obtained from this instrument.

REFERENCES:

1. Einstein, A. *Ann. Physik*, **1905**, 17, 132.
2. Reniers, F.; Tewell, C. J. *Electron Spectrosc.* **2005**, 142, 1.
3. Kiss, T. et al. *Phys. Rev. Lett.* **2005**, 94, 057001.
4. Suga, S. et al. *Rev. Sci. Instrum.* **2010**, 81, 105111.
5. Chesneau, F. et al. *J. Phys. Chem. C* **2010**, 114, 7112
6. Groñbeck, H.; Curioni, A.; Andreoni, W. *J. Am. Chem. Soc.* **2000**, 122, 3843.
7. Gottschalck, J.; Hammer, B. *J. Chem. Phys.* **2002**, 116, 784.
8. Heister, K.; Zharnikov, M.; Grunze, M.; Johansson, L. S. O. *J. Phys. Chem. B* **2001**, 105, 4058.
9. Groñbeck, H.; Hañkkinen, H.; Whetten, R. L. *J. Phys. Chem. C* **2008**, 112, 15940.
10. Heiman, P.; van der Veen, J. J.; Eastman, D. E. *Solid State Commun.* **1981**, 38, 595.
11. Chaudhuri, A.; Lerotholi, T. J.; Jackson, D. C.; Woodruff, D. P.; Dhanak, V. *Phys. Rev. Lett.* **2009**, 102, 126101 1.
12. Heister, K.; Johansson, L. S. O.; Grunze, M.; Zharnikov, M. *Surf. Sci.* **2003**, 529, 36.
13. Puschnig, p. et al. *Science* **2009**, 326, 702.
14. Schwarz, W. H. E., *Angew. Chem. Int. Ed.* **2006**, 45, 1508.
15. Itatani, J. et al. *Nature* **2004**, 432, 867.
16. Brion, C. E.; Cooper, G.; Zheng, Y.; Litvinyuk, I. V.; McCarthy, I. E. *Chem. Phys.* **2001**, 270,
17. Repp, J.; Meyer, G.; Stojkovic, S. M.; Gourdon, A.; Joachim, C.; *Phys. Rev. Lett.* **2005**, 94, 026803.
18. Temirov, R.; Soubatch, S.; Neucheva, O.; Lassise, A. C.; Tautz, F. S. N. *J. Phys.* **2008**, 10, 053012.
19. Damascelli, A. *Phys. Scr.* **2004**, T109, 61.
20. Feibelman, P. J.; Eastman, D. E. *Phys. Rev. B* **1974**, 10, 4932.

21. Gadzuk, J. W. *Phys. Rev. B* **1974**, *10*, 5030.
22. Koch, N. *et al. Phys. Rev. Lett.* **2006**, *96*, 156803.
23. Kakuta, H. *et al. Phys. Rev. Lett.* **2007**, *98*, 247601.
24. Berkebile, S. *et al. Phys. Rev. B* **2008**, *77*, 115312.
25. Tiago, M. L.; Northrup, J. E.; Louie, S. G. *Phys. Rev. B* **2003**, *67*, 115212.
26. Hummer, K.; Ambrosch-Draxl, C. *Phys. Rev. B* **2005**, *72*, 205205.
27. Nabok, D. *et al. Phys. Rev. B* **2005**, *76*, 235322.
28. Koini, M. *et al. Thin Solid Films* **2008**, *517*, 483.
29. Broekman, L. *et al. J. Electron. Spectrosc. Relat. Phenom.* **2005**, *144–147*, 1001.
30. Kiss, T. *et al., J. Electron Spectrosc. Relat. Phenom.* **2005**, *953*, 144.
31. Gorgoi, M.; Svensson, S.; Schäfers, F.; Öhrwall, G.; Mertin, M.; Bressler, P.; Karis, O.; Siegbahn, H.; Sandell, A.; Rensmo, H.; Doherty, W.; Jung, C.; Braun, W.; Eberhardt, W. *Nucl. Instrum. Meth.* **2009**, *48*, A 601.
32. Öhrwall, G. *et al. Journal of Electron Spectroscopy and Related Phenomena* **2011**, *183* 125.